Molecular Physics of Jumping Nanodroplets

(Electronic Supplementary Information submitted to *Nanoscale*)

Sreehari Perumanath*, Matthew K. Borg†
School of Engineering, University of Edinburgh, Edinburgh EH9 3FB, UK

James E. Sprittles‡
Mathematics Institute, University of Warwick, Coventry CV4 7AL, UK

Ryan Enright§
Thermal Management Research Group, ηET Dept., Nokia Bell-Labs, Dublin D15 Y6NT, Ireland

1 MD simulation details

Molecular dynamics (MD) simulations [1] of water and argon nanodroplets coalescing on superlyophobic surfaces are performed in order to study the effects of gas rarefaction and molecular thermal motion on the coalescence-induced jumping speed. MD is a deterministic, particle based simulation tool in which the time evolution of a set of interacting particles is carried out by integrating Newton's equations of motion: $\vec{F}_j = m_j \vec{a}_j$, where $\vec{F}_j$ is the net force on an atom j, m_j is its mass and $\vec{a}_j$ is the acceleration. The force on any atom is obtained by taking the negative gradient of the potential energy function due to all its neighbours.

Two different types of droplets are considered in the present study. The first set included two water droplets in near-vacuum/nitrogen atmosphere coalescing on top of a superlyophobic surface. For reasons of computational efficiency, water is modelled using the *mW mono-atomic water model* [2]. Here, each water molecule is modelled as a single atom and the interactions among these atoms are described by a Stillinger-Weber potential with potential parameters fine tuned to match the fluid properties of real water. The vapor pressure of this model at 300 K is negligible. In order to study the effect of outer gas on jumping speed, a single-site nitrogen (N) model is introduced, which uses the standard Lennard-Jones (LJ) potential to describe the inter-atomic interactions [3]:

$$U_{jk} = 4\epsilon_{jk} \left[\left(\frac{\sigma_{jk}}{r_{jk}} \right)^{12} - \left(\frac{\sigma_{jk}}{r_{jk}} \right)^{6} \right], \tag{1}$$

where ϵ_{jk} is the van der Waals interaction energy between the atoms, σ_{jk} is the length parameter and r_{jk} is the distance between the atoms ($\epsilon_{\mathrm{NN}} = 0.189$ kcal/mol, $\sigma_{\mathrm{NN}} = 0.375$ nm, $\epsilon_{\mathrm{mW-N}} = 0.13$ kcal/mol and $\sigma_{\mathrm{mW-N}} = 0.324$ nm). A cut-off distance of $r_c = 1.3$ nm is used in the present study and Lorentz-Berthelot mixing rules are employed to determine the cross-species interaction parameters.

---

*sreehari.dharmapalan@ed.ac.uk
†matthew.borg@ed.ac.uk
‡j.e.sprittles@warwick.ac.uk
§ryan.enright@nokia-bell-labs.com

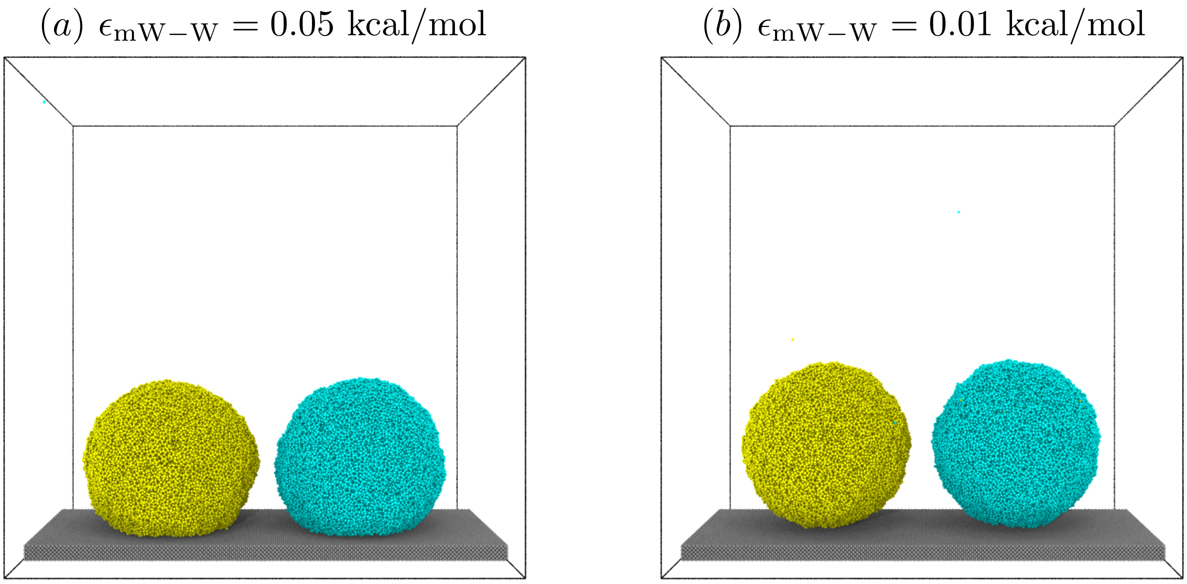

Figure S1: (a) Starting the simulations with two mW water droplets on top of a 'slightly' lyophobic wall. (b) The same droplets after the wall-liquid interaction potential is lowered to create a superlyophobic wall. We use a system-specific value of ϵ between wall and the fluid: $\epsilon_{\mathrm{mW-W}} = 0.01$ kcal/mol and $\epsilon_{\mathrm{Ar-W}} = 0.02$ kcal/mol.

In the second set of simulations, argon (Ar) droplets are simulated at 85 K in pure vapor. The interactions between any two atoms is also modelled by an LJ potential with $\epsilon_{\mathrm{ArAr}} = 0.238$ kcal/mol, $\sigma_{\mathrm{ArAr}} = 0.34$ nm and $r_c = 0.851$ nm. The thermophysical properties of different fluids used in the simulations are provided in the table below.

Description	Value
mW density	~ 1000 kg/m^3
mW viscosity	310 μPa-s [4]
mW specific heat capacity	1833 J/kgK [2]
mW surface tension	65.4 mN/m [2]
Nitrogen density	$0 - 22$ kg/m^3
Nitrogen viscosity ($T = 300$ K)	17.2 μPa-s
Argon (liquid) density	~ 1410 kg/m^3
Argon (liquid) viscosity	210 μPa-s
Argon surface tension	8.3 mN/m
Argon (vapor) density	~ 14 kg/m^3
Argon (vapor) viscosity ($T = 85$ K)	6.4 μPa-s

We begin the simulation by constructing a single droplet of a specified number of molecules according to the intended size R. This droplet is equilibrated in pure-vapor conditions for a long time and the relevant data such as positions and velocities of atoms are stored during the course of this run. Two unique random frames from this set are then taken and are placed on top of a wall to obtain the initial condition of our system.

Underneath the droplets, a wall is placed with FCC crystal structure and lattice parameter $a = 0.392$ nm. The interaction between fluid and wall atoms (W) are modelled using the LJ potential. The thickness of the wall is chosen to be the fluid-wall cut-off distance. We initially start the simulation with the two liquid droplets sitting on a 'slightly' lyophobic wall (see Fig. S1(a)). Then, the energy parameter between the wall and liquid atoms in the LJ potential is gradually reduced in small steps so that the contact angle between them increases well above 150° (see Fig. S1(b)). The full system is then equilibrated further for 5 ns. During the equilibration stage, a Berendsen thermostat is applied to the droplets and the time-integration is performed using a velocity-Verlet algorithm with a time-step size of 0.01 ps for water-based systems and 0.004 ps for argon-based systems. In all cases, the wall atoms are frozen to their initial lattice coordinates.

After both droplets are equilibrated for a long time, an impact speed of 2 m/s (sufficiently small to avoid having any influence on the jumping dynamics [5]) is given to them towards each other so that they will come together and coalesce. No thermostat is applied to the fluid during coalescence in order to avoid biasing the molecular dynamics. This procedure is repeated, and many realisations are performed for any single case in order to obtain statistically reliable results. Jumping speed is defined as the instantaneous centre-of-mass speed of the final droplet in the direction normal to the wall at the moment it loses contact with the wall. Water droplets of sizes $R = 3.1$, 4.2, 5.1, 7.2 and 15.1 nm, and argon droplets of sizes $R = 8.4$, 13.3, 23.1 and 55.2 nm are simulated in the present study.

2 VoF simulation details

Numerical simulations.— To study droplet coalescence and subsequent jumping on an ideal superlyophobic surface, we simulate the case of symmetric binary coalescence using the volume-of-fluid (VoF) approach with custom user-defined function for automated mesh adaption in order to well resolve the liquid/gas interface implemented in a finite-volume solver (Fluent v17.0, Ansys Inc.).

A uniform structured grid is used as the parent mesh. Three levels of adaption (cell splitting) are allowed providing for a minimum cell volume (V_{min}) in the interface region with characteristic length ($V_{min}^{1/3}$) of 1.9% the initial droplet radius, R. To simulate an ideal, non-wetting surface, the droplet wetting wall is assigned a single valued contact angle of $\theta_c = 180°$. Due to symmetry, only one quarter of the domain is simulated with dimensions of $3R \times 3R \times 5R$. The simulation domain is bounded by two symmetry planes dissecting the droplets where, by definition, the contact angle is constant at $\pi/2$; two boundaries specified with a shear-stress free condition (on the gas); the droplet wetting wall specified as no-slip (which still permits contact line motion, due to the 180° contact angle) and a single valued contact angle (contact angle hysteresis neglected); and an outlet vent, with the backflow direction specified from the neighbouring cell in the flow domain, opposite to the droplet wetting wall.

The droplet volume is patched into the simulation domain with a geometry corresponding to the droplets just in contact. The limited grid resolution led to an initial bridge radius of $\approx 0.1R$ that initiated the start of coalescence at $t = 0$. The properties of the liquid droplet, the surrounding gas and the interface between them are nominally those of water and humid air at room temperature (argon and argon vapor at 85 K), which corresponds to a nominal viscosity ratio, density ratio and surface tension of $\mu_l/\mu_g = 56$ (40) and $\rho_l/\rho_g = 815$ (307), $\gamma = 65.4$ (8.3) mN/m respectively. To simulate other viscosity ratios, the gas side viscosity is modified accordingly. The density ratio is kept fixed at the nominal base value for each simulation.

Discretization for pressure, momentum and volume fraction is done with the PRESTO!, QUICK and Geo-Reconstruct algorithms, respectively. The PISO algorithm is used for pressure-velocity coupling. The continuum surface force (CSF) model is used to capture the contribution of surface tension to the normal stress on the interface [6]. The VoF implementation is intrinsically volume conserving [7]. This is confirmed for all simulations by tracking the volume of the droplet phase during the simulations. The liquid-vapor interface is implicitly represented by the VoF function, which varies rapidly over a short distance, approximately the mesh cell

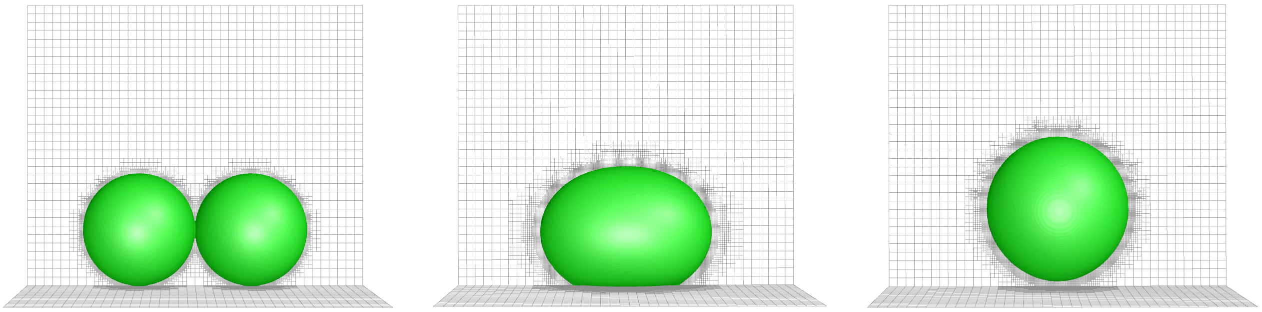

(a) $t/\tau = 0$ (b) $t/\tau = 1.93$ (c) $t/\tau = 4.5$

Figure S2: Volume-of-fluid simulation snapshots of two water droplets with $R = 7.2$ nm ($\mathrm{Oh}_l = 0.45$) coalescing and jumping when the viscosity ratio is small (i.e. jumping in the vacuum limit). Here, $\tau \equiv \sqrt{\rho_l R^3/\gamma}$ is the inertial-capillary time scale.

size. This abrupt change of the VoF function creates errors in calculating the normal vectors and the curvature of the interface used to evaluate the interfacial forces. These errors induce non-physical parasitic currents in the interfacial region, e.g. spurious velocities. Good results in reducing spurious velocities are obtained by using Fluents native smoothing function. One fully-weighted cycle of smoothing at each iteration is found to be suitable for the simulations. Under-smoothing, by reducing the weighting for a single smoothing cycle, led to noisy results and, in some cases, droplets that would begin accelerating after contact with the surface had been lost. Over-smoothing should also be avoided as this unphysically reduces the local curvature of the bridging region leading to a reduction in the simulated jumping speed. Adaptive time stepping was used to control the progression of the simulation. An initial period of 10 constant time steps ($t/\tau \leq 1 \times 10^{-2}$) was followed by varying time steps maintaining the global Courant number of 0.5. At the same time, the mesh was adapted every 10 time steps. This ensured that the interface never left the region of highest refinement during the simulation. Figure S2 shows typical VoF simulation snapshots during coalescence of two $R = 7.2$ nm droplets.

Determination of jumping speed from simulations.— Droplet jumping speeds are determined from simulations by calculating the mass-averaged droplet velocity when the droplet lost contact with the surface. It should be noted that, during the coalescence process, the droplet typically loses contact with the substrate twice. The first instance occurs during the initial bridge development where the entrainment liquid from the droplet bulk into the developing bridge region results in loss of contact with the substrate. As the liquid bridge expands, it eventually impacts the substrate leading to a substantial increase in the wetted area of liquid on the substrate. The point of departure was found to correlate well with normal force on the wall reaching a local negative maximum. An alternative definition of the jumping speed could be determined as when the droplet lost viscous communication with the wall after the local negative maximum normal force on the wall marked by a decay to zero transient force on the wall. This definition coincides with the observed start of a smooth linear decay in droplet velocity due primarily to drag with the surrounding fluid. The two definitions of jumping speed converge as the viscosity ratio approaches zero.

Curve fit for Oh_{lc} *data.*— A cut-off Oh_{lc} is defined as the minimum Oh_l at which the VoF simulations predict no jumping occurs. The inset of Fig. 1d of the manuscript shows the dependence of Oh_{lc} on the viscosity ratio $\mu_r \equiv \mu_g/\mu_l$. As the gas viscosity is reduced considerably below that of the coalescing liquid, it will become increasingly ‘passive’ and the dynamics is solely governed by the properties of the coalescing liquid. Consequently, the jumping speeds should asymptote to those in vacuum as μ_r is decreased. This feature is qualitatively captured by VoF simulations. The data from our VoF simulations are fit to a curve of the form:

$$\mathrm{Oh}_{lc} = A\left(1 - e^{-\left(\frac{\ln \mu_r}{B}\right)^C}\right) + D, \tag{2}$$

where the fitting parameters $A = 2.458,\ B = 6.591,\ C = 2.361$ and $D = 0.043$ with coefficient of determination $r^2 = 0.999$. While the above equation gives $\mathrm{Oh}_{lc} = D$ when $\mu_r = 1$ (i.e. when both coalescing liquid and the outer medium have identical viscosities, as shown previously [8]), it also asymptotes to a finite positive value $A + D = 2.501$, as $\mu_r \to 0$ (i.e. in the vacuum limit, as studied here). Eq. 2 is plotted in the inset of Fig. 1d of the manuscript.

3 Jumping speed in vacuum

We begin with the most simple case when two nanodroplets coalesce in vacuum, where the process is adiabatic. This will allow us to isolate the coalescing liquid's dynamics during the process, so that a comparison with coalescence in gas will help us identify the role of the gas.

When two droplets coalesce, energy is released as the total interfacial area decreases. A portion of this energy released is dissipated due to viscosity of the coalescing droplets (E_μ). The remaining portion of the total energy budget is utilised to overcome the adhesion from the surface (W_{adh}), generate a flow field inside the droplet after coalescence that does not contribute to jumping ($E_{\mathrm{circulation}}$) and convert it into the kinetic energy (KE) of the final droplet (if it jumps off the symmetry breaking superlyophobic surface), i.e.

$$\gamma \Delta A = W_{\mathrm{adh}} + W_{\mathrm{flow}}, \tag{3}$$

where

$$W_{\mathrm{flow}} = E_\mu + \mathrm{KE} + E_{\mathrm{circulation}}, \tag{4}$$

γ is the interfacial tension and $\Delta A = 4\pi R^2(2 - 2^{2/3})$ is the reduction in the surface area due to coalescence, where we assume a sphere is rapidly formed. Furthermore, in the next section, we show $W_{\mathrm{adh}} \sim KE$.

At the point where the droplet leaves the surface along its trajectory, W_{flow} is composed of the viscously dissipated flow component E_μ, the translational kinetic energy KE, and what is left of the flow within the droplet, $E_{\mathrm{circulation}}$, following jumping that is viscously dissipated quickly after the jump point. The energy spent due to viscous dissipation results in an increase in the average temperature over the entire coalescing droplets and is given by $2m_d c_p \Delta T_v$, where $m_d = 4\pi R^3 \rho_l / 3$ is the mass of a single droplet of radius R with density ρ_l before coalescence, c_p is the specific heat capacity of the coalescing liquid, $\Delta T_v = T_{jump} - T_{initial}$ is the temperature rise when droplets coalesce, with subscript 'v' representing processes occurring in vacuum, T_{jump} is the temperature of the final droplet when it takes off the non-wetting surface and $T_{initial}$ is the initial temperature of the smaller droplets. In Fig. 2(c) of the main Letter, the variation of temperature with time during coalescence of two water nanodroplets and the corresponding simulation snapshots are shown. Notably, temperature is far easier to measure in MD than directly computing viscous dissipation from gradients of the flow fields. For nanodroplets, the coalescence process is largely viscous dominated and by noticing that the temperature of the final droplet does not increase appreciably after coalescence has completed, we assume the energy associated with the circulatory flow field inside the droplets to be negligible ($E_{\mathrm{circulation}} \approx 0$). So Eq. 3 changes to

$$\gamma\left[4\pi R^2(2 - 2^{2/3})\right] = W_{\mathrm{adh}} + 2m_d c_p \Delta T_v + m_d V_v^2. \tag{5}$$

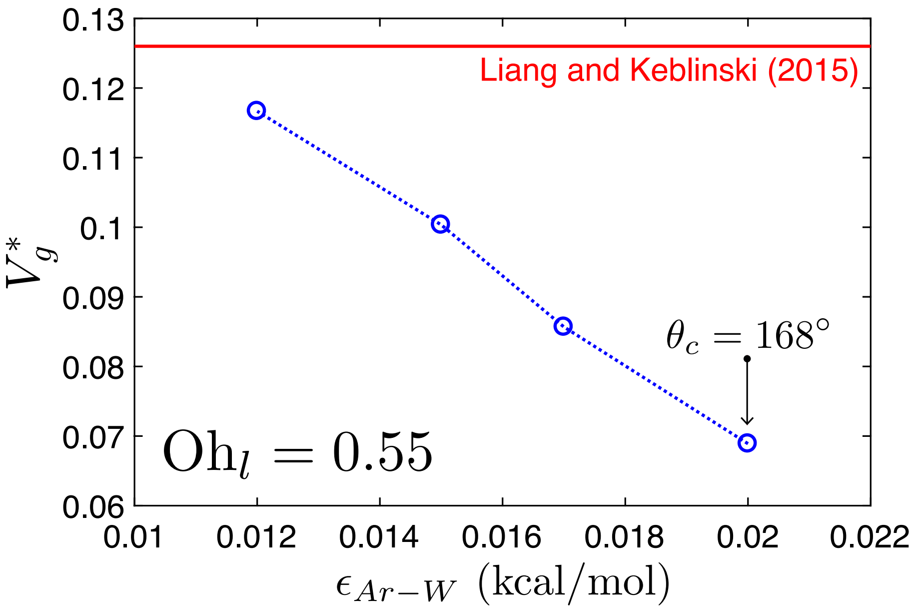

Figure S3: The effect of wall wettability on the jumping speed for coalescing argon droplets ($R = 13.3$ nm). The results of Ref. [5] is reproducible at lower ϵ_{Ar-W}. For argon droplets in our simulations, $\epsilon_{Ar-W} = 0.02$ kcal/mol is used in order to avoid complications due to increased thermal fluctuations.

Rearranging the terms gives:

$$\Delta T_v = \left(1.24 - V_v^{*2} - \frac{W_{\mathrm{adh}}}{m_d U^2}\right) \frac{(\gamma/\mu_l)^2}{2c_p} \mathrm{Oh}_l^2. \tag{6}$$

In the above equation, $V_v^* = V_v/U$ is the jumping speed in vacuum normalised with the inertial-capillary velocity scale $U = \sqrt{\gamma/\rho_l R}$, and $\mathrm{Oh}_l = \mu_l/\sqrt{\rho_l \gamma R}$ is the Ohnesorge number based on liquid properties, where μ_l is the dynamic viscosity. With $V_v^{*2} \ll 1$, $W_{\mathrm{adh}} \sim KE$ and the properties of mW water as given in the table above, Eq. 6 simplifies to $\Delta T_v(K) \approx 15\ \mathrm{Oh}_l^2$, so that as one would expect, viscous dissipation increases as the 'dimensionless viscosity (Oh_l)' increases. In Fig. 2(d) of the main Letter, the temperature rise measured from our MD simulations is compared with the above equation, and their closeness validates the assumptions made.

4 Jumping speed in presence of a rarefied gas

The relevant physics may be different if we have a surrounding gas/vapor in the system. Since the surface tension (γ) is a weak function of the pressure outside the droplets (p_∞), the total energy budget of the system in the presence of a gaseous atmosphere can be assumed to be the same as that in the absence of it. However, during the coalescence process, a part of the energy budget is spent in order to overcome the drag from the ambient gas. The energy balance in this case is:

$$\gamma \Delta A = W_{\mathrm{adh}} + 2 m_d c_p \Delta T_g + m_d V_g^2 + W_{\mathrm{drag}}, \tag{7}$$

where ΔT_g is the increase in temperature of the droplets (subscript g denotes 'in the presence of gas'), V_g is the final droplet jumping speed and W_{drag} is the work done against drag during the time both droplets coalesce.

We perform MD simulations on argon droplets to carefully determine the share of W_{adh} in the overall energy balance. Out of various factors that defines the coalescence-induced jumping

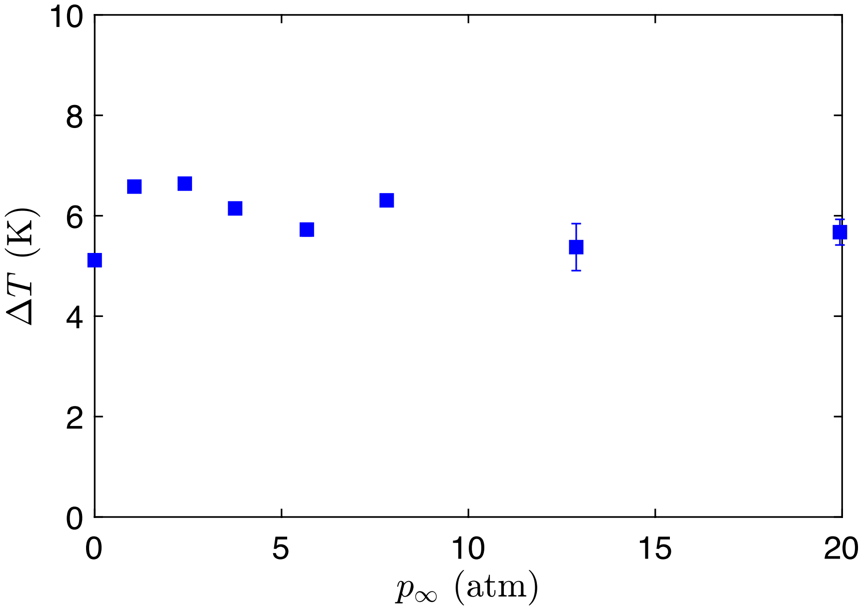

Figure S4: Temperature rise during coalescence of two water nanodroplets with $R = 5.1$ nm as a function of ambient pressure. ΔT is essentially independent of p_∞.

speed of nanodroplets from superlyophobic surfaces, adhesion from the substrate and contact angle hysteresis, which stem from the wettability of the underlying substrate, play crucial roles and have already been studied for nanodroplets in the past [9–11]. For example, Sheng et al. [10] observed larger adhesion and higher contact angle hysteresis on surfaces with higher wettability, which is reflected in the reduced jumping speed of the coalesced nanodroplet. Here, we quantify the relative magnitudes of W_{adh} and KE in order to investigate their respective contributions to the energy balance.

Figure S3 shows the variation of scaled jumping speed as a function of wall-argon energy interaction parameter, ϵ_{Ar-W}. Since the major effect of adhesion is in changing the jumping speed by a factor of ~ 1 in the range of ϵ_{Ar-W} investigated (where θ_c is well above 150°), we conclude that $W_{\mathrm{adh}} \sim KE$. We find that smaller droplets lose contact with the wall at low values of ϵ, due to increased effects of thermal fluctuations. Furthermore, we assume W_{adh} is independent of the outer conditions, as we observe no discernible changes in the coalescing droplet geometry during the process (see supporting video and Fig. S8 below).

From our MD simulations, we observe that $\Delta T_g \approx \Delta T_v$ (see Fig. S4), indicating that the internal viscous dissipation during the coalescence of nanodroplets is not drastically affected by the presence of a gaseous medium outside, i.e. heat transfer from the liquid to the outer gas phase is negligible over the time-scale of the process.

In order to characterise the effect of drag from the outer gas on the jumping speed, we define a Knudsen number based on the mean-free-path of the surrounding gas and the droplet radius, i.e. $\mathrm{Kn} = \lambda / R$. Here we evaluate the mean-free-path of the surrounding gas using the relationship between λ and viscosity of the gas (μ_g):

$$\lambda = \frac{\mu_g}{p_\infty}\sqrt{\frac{\pi k_B T}{2m}}, \tag{8}$$

where m is the mass of a single gas molecule.

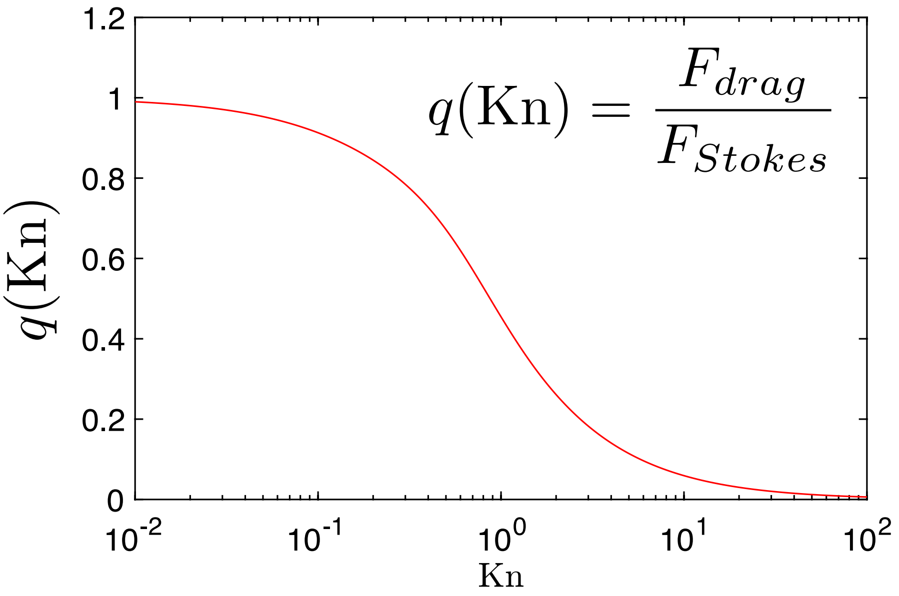

Figure S5: Variation of drag on small spheres for a wide range of Kn.

4.1 Drag on coalescing droplets

Estimating W_{drag} in Eq. 7 is challenging. The ideal way of estimating W_{drag} during coalescence is by explicitly determining the total stress causing drag over the entire surface and summing the work done against it over the time scale of droplet coalescence. However, evaluating local stress tensors on the droplet surface in nanoscale systems is highly challenging because (a) thermal fluctuations are strong, (b) there can be slip across interfaces and (c) the process happens very rapidly. In what follows, we try to establish a crude estimate, which captures some of the underlying physics of the work done against the drag during coalescence-induced jumping of nanodroplets.

For a small rigid, spherical particle of radius a, moving through a highly viscous infinite medium (μ_g), with a relative speed v at low particle Reynolds number, the Stokes drag force experienced by it is given by

$$F_{Stokes} = 6\pi\mu_g a v, \tag{9}$$

which is accurate only when the Knudsen number (based on particle radius) is small. In the coalescence-induced jumping problem that we study, the drag will be different from the above expression due to three main reasons: (a) because of the rarefaction in the surrounding gas resulting in finite non-zero particle Kn, (b) due to the influence of the wall under both droplets and (c) due to the complex flow geometry during the coalescence process. We consider each of these problems in detail below.

(a) *Modification due to finite non-zero* Kn— In this case, the slip between the particle surface and the ambient medium must be accounted for, while evaluating the drag force on it. There have been many attempts to incorporate slip at interfaces into the Stokes-flow analysis and one of the most successful ones for determining the drag force on small spheres moving through a gas, without any restrictions on Kn, is by Warren F. Phillips [12]. His approximate theoretical expression gives

$$F_{drag} = F_{Stokes} q(\mathrm{Kn}) = 6\pi\mu_g a v \left(1 - \frac{15\mathrm{Kn} - 15.42\mathrm{Kn}^2 + 54\mathrm{Kn}^3}{15 + 12\mathrm{Kn} + 18\mathrm{Kn}^2 + 54\mathrm{Kn}^3}\right), \tag{10}$$

where q is a correction factor incorporating the effects of gas rarefaction on a moving spherical particle in an infinite medium. Figure S5 shows how the drag force on a small sphere gets

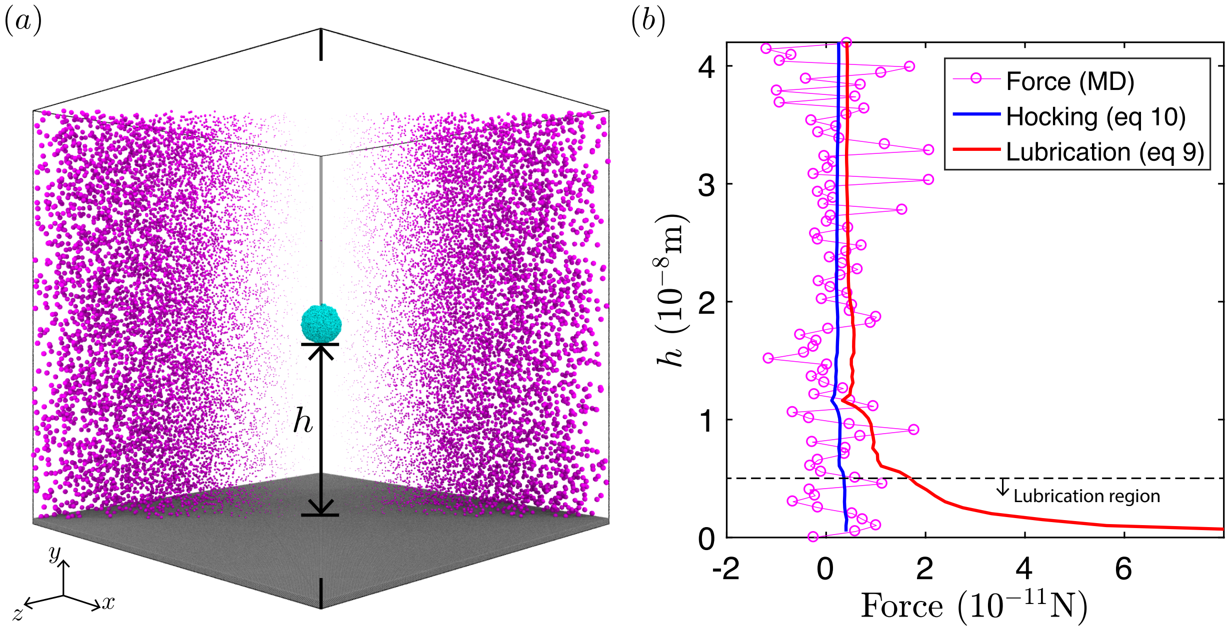

Figure S6: (a) Slice of the MD domain used in this section to study drag on a spherical nanodroplet approaching a wall (water droplet of $R = 5.1$ nm in nitrogen atmosphere at Kn $= 3.7$). (b) Comparison of drag obtained from MD simulations with Hocking drag and drag derived from lubrication approximation. Force is calculated using the instantaneous speed of the sphere at each vertical location. While the latter diverges for the droplet near the wall, Hocking's expression seems to better capture the physics even for such nanoscale systems.

modified for a wide range of particle Kn [12]. In our analyses, we assume complete accommodation (i.e. purely diffuse reflection) between water droplets and nitrogen molecules. The above equation is derived by assuming that the mean speed is much less than the thermal speed of particles in the surrounding medium, which is the case when the final droplet jumps off the superlyophobic surface.

(b) *Modification due to the presence of wall (sphere approaching a wall)*— When a particle approaches a wall, the classical analysis based on the lubrication approximation predicts that the opposing force is inversely proportional to the gap (h) between the particle and the wall [13], i.e.

$$F_{Lubrication} = F_{Stokes}\phi_L = 6\pi\mu_g av\left(\frac{a}{h}\right), \tag{11}$$

for large values of ϕ_L. This would mean that, for a finite downward force (e.g. due to gravity), a contact is impossible in finite time.

Hocking [13] used Maxwell's slip boundary condition to quantify the resisting force between approaching surfaces and found that the force depended only logarithmically on the gap width between the surfaces, in which case a contact can be achieved in finite time. His analysis gives:

$$F_{Hocking} = F_{Stokes}\phi_H = 6\pi\mu_g av\left(\frac{2a}{h\eta^2}[(1+\eta)\log(1+\eta)-\eta]\right), \tag{12}$$

where $\eta \equiv 6\lambda/h$ is like a local Knudsen number.

Here, we perform a separate set of MD simulations in order to compare the force experienced by a droplet moving towards a wall with that predicted by the Hocking and lubrication expressions for the resisting force. Figure S6(a) shows the geometry used for this separate analysis and in Figure S6(b), we compare the forces. We equilibrate a system containing a water droplet of $R = 5.1$ nm in a nitrogen atmosphere at $p_\infty = 3.75$ atm at $T = 300$ K for a long

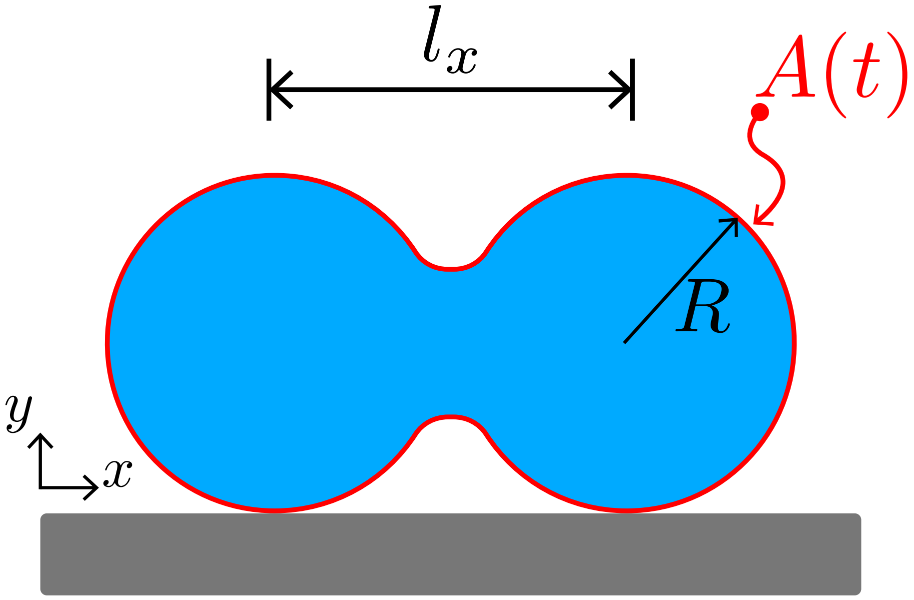

Figure S7: Schematic of the coalescence process for determining the work done against drag during droplets coalescence.

time ($\sim$ 5 ns) and apply an impact speed of 20 m/s (of the order of maximum jumping speed observed in our simulations) to the droplet towards the wall from a height of 50 nm above the wall. For the droplet near the wall, we explicitly measure the force on it in a direction normal to the wall due to all surrounding gas molecules as a function of the gap width h. While the classical analysis based on lubrication approximation wildly over-predicts the opposing force in the lubrication region ($h < 5$ nm), the reduction factor ϕ_H helps Hocking's expression to follow the variation of the force observed in nanoscale droplets.

The above two expressions are derived for a simpler flow geometry than what we have when two droplets coalesce and jump. Consequently, it may not be appropriate to use any of them, even Hocking's expression, in determining the effect of wall on the drag on droplets as they merge. Nevertheless, we note that depending on the problem at hand, some reduction factor (ϕ or q) modifies the Stokes drag on a spherical particle to account for slip at interfaces (in the simplest case) caused by kinetic gas effects; an exact theoretical expression without experimental fitting is not always available, even for some simple systems.

(c) *Modification due to complex flow geometry*— In order to evaluate the total work done against drag during the coalescence process, we decompose the drag into two components: the first being the drag on the droplets because of their motion towards each other in the direction parallel to the underlying wall as they coalesce ($W_{\parallel}$) and the second is due to their motion in the direction normal to the wall ($W_{\perp}$). Next, we will make some assumptions about how to model these two phases of the process in a manner that captures the main physics but remains as simple as possible to work its way into our theoretical equation (Eq. 7).

For evaluating $W_{\parallel}$, we equate the droplets' instantaneous total surface area $A(t)$ to that of two full spheres moving in an infinite ambient medium of viscosity μ_g, each with a speed relative to the ambient medium given by half the instantaneous speed of approach of the droplets: $V_x(t) = \Delta l_x/\Delta t$ (see Fig. S7). In moving both droplets towards each other by a distance Δx parallel to the wall, the infinitesimal amount of work done against the drag will be:

$$\Delta W_{\parallel} = 2\bigg(6\pi\mu_g a(t)\frac{V_x(t)}{2}q(\mathrm{Kn})\bigg)\frac{\Delta x}{2}, \tag{13}$$

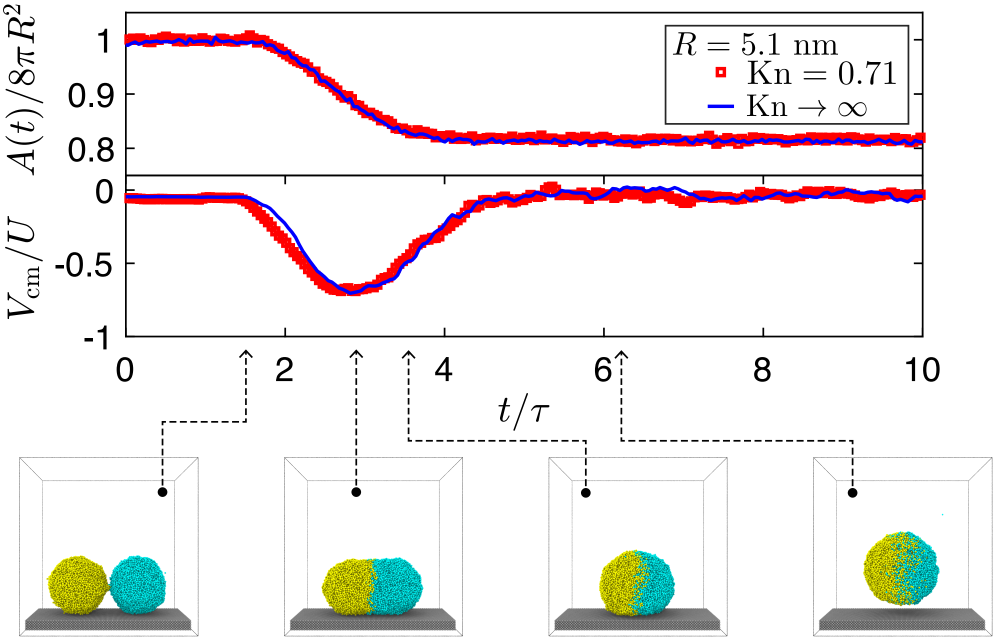

Figure S8: The time evolution of scaled total surface area and approach speed of the droplets during coalescence of two $R = 5.1$ nm droplets.

where $a(t) = \sqrt{A(t)/8\pi}$ is the radius of two full spheres as described above. Here we have used Eq. 10, since the coalescence happens in a finite non-zero Kn atmosphere.

Similarly, in order to evaluate $W_\perp$, the instantaneous total surface area is equated to a single sphere of the same area moving in the infinite ambient medium with a speed given by the instantaneous speed of coalescing droplets in y direction. Then, the work done against this drag will be:

$$\Delta W_\perp = \left(6\pi\mu_g\sqrt{2}a(t)|V_y(t)|q(\mathrm{Kn})\right)|\Delta y|. \tag{14}$$

Therefore, the total work done against drag during coalescence (W_{drag}) can be obtained by summing all the infinitesimal amounts of both contributions from the beginning of coalescence until it ends, multiplied by an unknown correction factor ψ that we introduce here in order to accommodate the effects of a complex deforming liquid body and any possible influence of the underlying wall on drag that is not considered in this simplified analysis. Obtaining an analytical expression for this correction factor will be difficult and so, ψ will determined later by curve fitting.

In Fig. S8, the time evolution of the scaled total surface area and the approach speed are shown for $R = 5.1$ nm droplets. $\mathrm{Kn} \to \infty$ denotes simulations in vacuum. As we have already seen, the dynamics is nearly unaffected by the presence of an ambient gaseous medium and the coalescence process at such high Oh_l is 'smooth', as there are no obvious oscillations in any of the measured quantities. In the figure, we determine $A(t)$ in MD simulations using a method described in one of our previous studies [14]. Figure S9 shows how the centre-of-mass speed in the direction normal to wall changes as coalescence proceeds for $R = 7.2$ nm droplets. The major change in the dynamics occurs only towards the end, where droplets have already merged and the final droplet is about to lift-off from the surface. Since we are interested in how the jumping speed gets modified relative to its value in the limiting vacuum case, we evaluate drag in all cases by using $V_y(t)$ corresponding to the vacuum case. Hence, we have only one fitting parameter in the entire analysis: ψ.

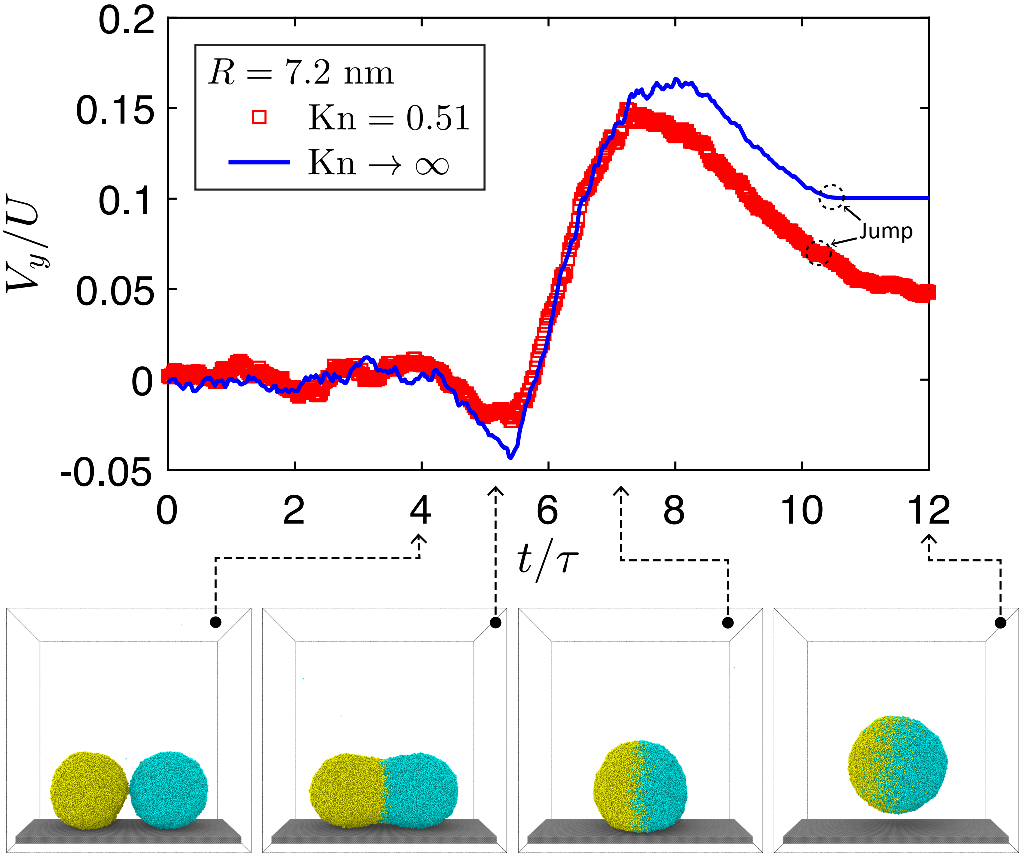

Figure S9: The time evolution of centre-of-mass speed of the droplets ($R = 5.1$) in the direction normal to the wall at two representative outer conditions. The presence of an outer fluid changes the behaviour of V_y, especially towards the end of the coalescence process. Simulation snapshots show the coalescence in vacuum.

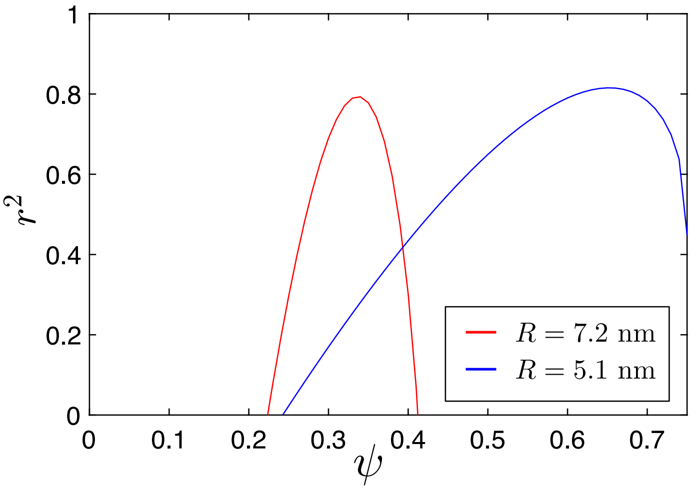

Figure S10: Variation of the coefficient of determination with the correction factor ψ for droplets with $R = 5.1$ nm and $R = 7.2$ nm.

Equating Eq. 5 to Eq. 7 by setting $\Delta T_g \approx \Delta T_v$, the energy balance will then reduce to

$$m_d V_g^2 = m_d V_v^2 - W_{\text{drag}}. \tag{15}$$

Dividing both sides by $m_d U^2$ and subsequent modification gives,

$$V_g^* = \sqrt{V_v^{*2} - \frac{W_{\text{drag}}}{m_d U^2}} = \sqrt{V_v^{*2} - \frac{\psi \sum(\Delta W_\perp + \Delta W_\parallel)}{m_d U^2}}. \tag{16}$$

In the above equation, as mentioned before, the summation is performed over the timescale of coalescence, i.e. from the moment two droplets touch till the final droplet lifts off. It must be noted that although the above equation provides reasonable insights about the process, it requires the knowledge of V_v^* to obtain V_g^*.

In Figs. 2(a) and 2(b) of the main Letter, the scaled jumping speed as a function of Kn is shown for two systems with $R = 7.2$ nm and $R = 5.1$ nm. For both cases, we fit the data to Eq. 16 with only the correction factor we introduced, ψ, as the fitting parameter. In Fig. S10, the coefficient of determination (r^2) obtained during curve fitting is plotted as a function of ψ. For both cases, that value of ψ which maximised r^2 is chosen to plot the red curves in Figs. 2(a) and 2(b) of the main Letter.

5 Nanodroplet bouncing on superlyophobic surfaces

Figure S11 shows the ‘bouncing’ of a nanodroplet on top of a superlyophobic surface due to thermal fluctuations. This effect is more predominant for smaller droplets, as the amplitude of surface thermal fluctuations are ~ 1 nm. The bouncing can also be clearly seen in the supporting video.

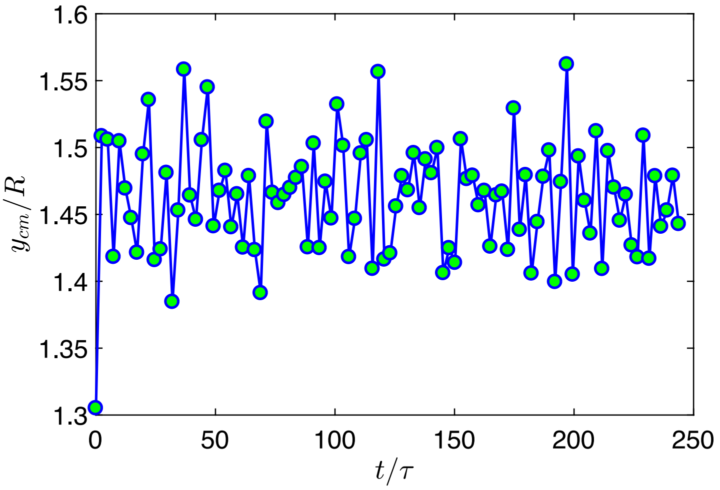

Figure S11: The y coordinate of centre-of-mass of a nanodroplet on a superlyophobic surface ($R = 3.1$ nm). Due to surface thermal fluctuations, the droplet 'bounces' up and down on a superlyophobic surface.

References

[1] Allen, M. P. and Tildesley, D. J. (2017) Computer Simulation of Liquids, Oxford University Press, New York 2 edition.

[2] Molinero, V. and Moore, E. B. (2009) Water Modeled As an Intermediate Element between Carbon and Silicon. *J. Phys. Chem. B,* **113**(13), 4008–4016.

[3] Coasne, B., Galarneau, A., Di Renzo, F., and Pellenq, R. J. M. (2010) Molecular Simulation of Nitrogen Adsorption in Nanoporous Silica. *Langmuir,* **26**(13), 10872–10881.

[4] Dhabal, D., Chakravarty, C., Molinero, V., and Kashyap, H. K. (2016) Comparison of liquid-state anomalies in Stillinger-Weber models of water, silicon, and germanium. *J. Chem. Phys.,* **145**(21), 214502.

[5] Liang, Z. and Keblinski, P. (2015) Coalescence-induced jumping of nanoscale droplets on super-hydrophobic surfaces. *Appl. Phys. Lett.,* **107**(14), 0–5.

[6] Hirt, C. and Nichols, B. (1981) Volume of fluid (VOF) method for the dynamics of free boundaries. *J. Comput. Phys.,* **39**(1), 201 – 225.

[7] Brackbill, J., Kothe, D., and Zemach, C. (1992) A continuum method for modeling surface tension. *J. Comput. Phys.,* **100**(2), 335 – 354.

[8] Lei, S., Wang, N., Liu, H., Nolan, K., and Enright, R. (jul, 2015) 2D Lattice Boltzmann Simulation of Droplet Jumping in a Viscous Fluid. In *ASME 2015 13th International Conference on Nanochannels, Microchannels, and Minichannels* American Society of Mechanical Engineers pp. 1–8.

[9] Cha, H., Xu, C., Sotelo, J., Chun, J. M., Yokoyama, Y., Enright, R., and Miljkovic, N. (Oct, 2016) Coalescence-induced nanodroplet jumping. *Phys. Rev. Fluids,* **1**, 064102.

[10] Sheng, Q., Sun, J., Wang, W., Wang, H. S., and Bailey, C. G. (2017) How solid surface free energy determines coalescence-induced nanodroplet jumping: A molecular dynamics investigation. *J. Appl. Phys.,* **122**(24), 245301.

[11] Gao, S., Liao, Q., Liu, W., and Liu, Z. (2018) Coalescence-Induced Jumping of Nanodroplets on Textured Surfaces. *J. Phys. Chem. Lett.,* **9**(1), 13–18.

[12] Phillips, W. F. (1975) Drag on a small sphere moving through a gas. *Phys. Fluids,* **18**(9), 1089–1093.

[13] Hocking, L. M. (1973) The effect of slip on the motion of a sphere close to a wall and of two adjacent spheres. *J. Eng. Math,* **7**(3), 207–221.

[14] Perumanath, S., Borg, M. K., Chubynsky, M. V., Sprittles, J. E., and Reese, J. M. (Mar, 2019) Droplet Coalescence is Initiated by Thermal Motion. *Phys. Rev. Lett.,* **122**, 104501.